ELSEVIER

1 April 1996

Optics Communications 125 (1996) 158–167

OPTICS COMMUNICATIONS

Full length article

Semiconductor laser confocal and interference microscopy

N.P. Rea, T. Wilson, R. Juškaitis

Department of Engineering Science, University of Oxford, Parks Road, Oxford OX1 3PJ, UK

Received 6 September 1995; accepted 14 November 1995

Abstract

We describe a semiconductor laser confocal microscope which has the capability to produce both confocal and interference images. This versatility is achieved by using different lasing regimes of the laser, which are controlled by its injection current. When operated just above threshold the coherence length of the laser is too short to allow interferometry so a pure confocal image is obtained. At higher injection currents the coherence length is sufficient to produce interference effects. We present an almost common path interference confocal microscope in which a single mode optical fibre is used both to launch and to detect the confocal signal as well as to provide the reference beam. To obtain surface profilometry we introduce a high frequency modulation to the semiconductor laser injection current which results in a corresponding modulation of the laser wavelength. We then use lock-in demodulation together with a simple feedback system to obtain the phase image and hence the surface profile. We also discuss the issue of resolution in phase imaging systems.

1. Introduction

A number of recent papers have been concerned with developing simple, compact, confocal microscopes with very low alignment tolerances. These systems, which have been reciprocal in nature, involve either the use of single mode optical fibres or direct laser feedback to detect the confocal image signal [1–4]. All these systems are able to produce three-dimensional images in the same way as traditional confocal microscopes. In order to increase the axial sensitivity and to obtain high resolution surface profilometry it is usual to adopt an interference approach. The image in this case consists of a superposition of a non-interference image together with an interference term image which is particularly sensitive to very small changes in optical path. It is often convenient to introduce some kind of phase modulation to either of the interfering beams so that the interference term image may be extracted electronically from the full image for further processing. It is worth remembering that the interference term image from an appropriately designed conventional interference microscope is identical to that obtained in a confocal system and so, in principle, these images may be used to produce both high resolution surface profilometry and confocal imaging [5,6]. However these systems are usually quite difficult to align and so it is of interest to ask if any of the new designs of confocal microscope can be easily modified to provide both confocal and interference imaging.

As we have said it is necessary to introduce a relative phase modulation in order to extract the interference term image. This may be achieved mechanically, which is usually slow, or electro-optically which involves the use of a bulky, high voltage, element [7,8]. An alternative method is to use a semiconductor laser as the light source and to use injection current modulation to introduce the required phase modulation [9]. This approach has the advantage that no further optical elements need to be introduced into the system.

0030-4018/96/$12.00 © 1996 Elsevier Science B.V. All rights reserved
SSDI 0030-4018(95)00701-6

In the following we shall describe a confocal fibre optic interferometer [10] in which the phase modulation is achieved in this way. We note that this approach adds versatility in that pure confocal imaging rather than interference imaging results simply by reducing the injection current.

2. Preliminary considerations

The key elements of our optical system are shown in Fig. 1. The single mode fibre serves both to launch the light into the microscope and to detect the reflected confocal field *amplitude*, U. We do not index match the fibre tip to the microscope optics and so part of the incident light is reflected back along the fibre from the tip; this forms the reference beam of relative amplitude, r. Since both the object and reference waves propagate back along the fibre in the same mode their phase fronts are perfectly matched when they are permitted to interfere on the photodiode detector. The detected signal is given by

$$I = |r + U\exp(-2jkl)|^2, \quad (1)$$

where the phase factor $\exp(-2jkl)$ ($k = 2\pi/\lambda$ and λ represents the wavelength) has been introduced to take account of the relative phase difference between the two beams.

We note that the only non-common path part of the of the system is that between the fibre tip and the object. In order to separate out the interference term image, from the confocal image $|U|^2$ and the constant background $|r|^2$ we elect to modulate the injection current of the semiconductor laser harmonically such that the wavelength is also modulated harmonically. This permits us to write

$$k = k_0 + (\Delta k)\cos\omega t, \quad (2)$$

where k_0 is evaluated at the nominal laser wavelength, Δk represents the modulation depth and ω is the modulation frequency. We may now re-write Eq. (1) as

$$I = |r + U' \exp[-j\phi(t)|^2], \quad (3)$$

where $U' = U\exp(-2jk_0 l)$ and the phase $\phi(t)$ is given by

$$\phi(t) = 2(\Delta k) l \cos\omega t. \quad (4)$$

As we shall see later the actual value of Δk depends on the specific value of injection current modulation used. However it will suffice for the moment to take a typical value of, say, $2 \times 10^{-5}\ \mu m^{-1}$, which together with an optical length l of 16 cm shows that a phase modulation of the order of 2π radians can easily be achieved.

The confocal image field, U, is itself a function of wavelength via [11]

$$U \sim h^2 \otimes \tau, \quad (5)$$

where τ represents the object amplitude reflection coefficient, h is the amplitude point spread function and the symbol $\otimes$ denotes the convolution operation. The amplitude point spread function is given by [11]

$$h \sim k \int_0^1 P(\rho) \exp\left(j\,\frac{u\rho^2}{2}\right) J_0(v\rho)\,\rho\,d\rho, \quad (6)$$

where $P(\rho)$ represents the pupil function of the lens and J_0 is a zero order Bessel function of the first kind.

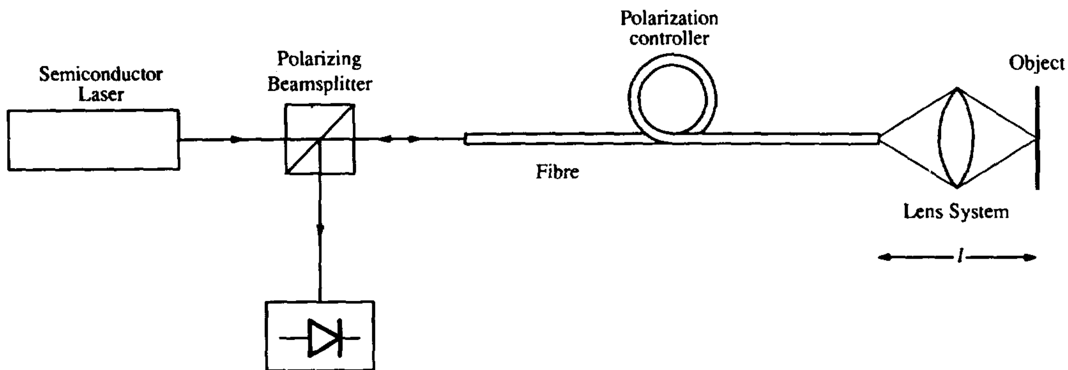

Fig. 1. Schematic diagram of the microscope optics.

The optical co-ordinates u and v are related to real axial co-ordinate z and radial co-ordinate r via

$$u=4kz\sin^2\alpha/2,\quad v=kr\sin\alpha, \tag{7}$$

where $\sin\alpha$ represents the numerical aperture.

We note that for the small value of Δk (10^{-5} μm^{-1}) in comparison with k_0 ($=7.97$ μm^{-1} for a 788 nm laser) it is reasonable to replace k by k_0 in the pre-multiplying factor and in the definitions of u and v. This is permissible even in the phase factor, $\exp(ju\rho^2/2)$, since the maximum value of $\exp[j2(\Delta k)\rho^2 z\cos\omega t \sin^2\alpha/2]$ is $\exp[j(\Delta k)z]$ for a numerical aperture of unity. We recall that z is likely to be in the micron region and so Δkz will always be very small so that it is reasonable to set $\exp[j(\Delta k)z]=1$.

We are now almost in a position to write an expression for the image intensity but we must first remember that modulating the injection current not only leads to a frequency modulation but also to an intensity modulation. If we include this effect in Eqs. (3) and (4) we obtain

$$\begin{aligned}I&=(1+\beta\cos\omega t)\,|r+U'\exp(-j\phi_0\cos\omega t)|^2\\&=(1+\beta\cos\omega t)\{r^2+|U|^2\\&\quad+2r[\mathrm{Re}\{U'\}\cos(\phi_0\cos\omega t)\\&\quad+\mathrm{Im}\{U'\}\sin(\phi_0\cos\omega t)]\},\end{aligned} \tag{8}$$

where $\mathrm{Re}\{U'\}$ and $\mathrm{Im}\{U'\}$ represent the real and imaginary part of U' respectively. We have introduced β to represent the intensity modulation and $\phi_0=2(\Delta k)l$. We have also assumed, for simplicity, that r is real.

We now recall that we may write $\exp(-j\phi_0\cos\omega t)$ as [12]

$$\begin{aligned}&\exp(-j\phi_0\cos\omega t)\\&\quad=\{J_0(\phi_0)-2J_2(\phi_0)\cos2\omega t+2J_4(\phi_0)\cos4\omega t\ldots\}\\&\quad-j\{2J_1(\phi_0)\cos\omega t-2J_3(\phi_0)\cos3\omega t\ldots\}.\end{aligned} \tag{9}$$

Since our intention is to extract the interference term image from Eq. (8) it is tempting to carry out synchronous demodulation. In essence this involves multiplying Eq. (8) by $\cos\omega t$ and time averaging the result. This is relatively straightforward to do and leads to a signal, I_ω of the form

$$\begin{aligned}I_\omega&\sim\beta[|U|^2+r^2]+2r[2J_1(\phi_0)\,\mathrm{Im}\{U'\}\\&\quad+\beta(J_0(\phi_0)-J_2(\phi_0))\,\mathrm{Re}\{U'\}],\end{aligned} \tag{10}$$

which may be recast as

$$I_\omega\sim\beta[|U|^2+r^2]+2rN|U|\sin[\mathrm{Arg}\{U\}-2k_0l+\delta], \tag{11}$$

where $\mathrm{Arg}\{U\}$ denotes the argument of U and the constants N and δ are given by

$$\sqrt{4J_1^2(\phi_0)+\beta^2(J_0(\phi_0)-2J_2(\phi_0))^2}$$

and

$$\tan^{-1}\{\beta[J_0(\phi_0)-J_2(\phi_0)]/[2J_1(\phi_0)]\}$$

respectively.

We can see that an undesirable side effect of the intensity modulation, β, is the presence of the confocal image, $|U|^2$, together with the required interference term image. We can overcome this drawback by performing the demodulation at a frequency, 2ω. In this case we obtain

$$I_{2\omega}\sim2J_2(\phi_0)\,\mathrm{Re}\{U'\}-\beta[J_1(\phi_0)-J_3(\phi_0)]\,\mathrm{Im}\{U'\}, \tag{12}$$

which may be recast as

$$I_{2\omega}\sim|U|\cos[\mathrm{Arg}\{U\}-2k_0l-\psi], \tag{13}$$

where the constant phase factor ψ is given by

$$\tan^{-1}\{\beta[J_3(\phi_0)-J_1(\phi_0)]/[2J_2(\phi_0)]\}.$$

This demodulated signal now represents the pure interference term image which consists of a fringe pattern superimposed on a confocal modulus image. We note that in this case the only effect of the intensity modulation has been to introduce a constant phase shift ψ into the fringe pattern.

It is now possible, in principle, to extract both $|U|$ and $\mathrm{Arg}\{U\}$ from the two demodulated signals I_ω and $I_{2\omega}$. However this is impractical because of the complicated form of I_ω, Eq. (11), and the need to accurately determine parameters such as β, r, ϕ_0. An alternative would be to introduce some additional, controllable, phase difference, $\Delta\phi$, between the object and reference beam such that Eq. (13) becomes

$$I_{2\omega}\sim|U|\cos[\mathrm{Arg}\{U\}-\Delta\phi-2k_0l-\psi] \tag{14}$$

and to use a feedback technique to set $\Delta\phi$ such that, at each picture point, the cosine term in Eq. (14) remained zero. In this way the variations in $\Delta\phi$ will be proportional to variations in $\mathrm{Arg}\{U\}$ since $2k_0l+\psi$ merely represents a constant phase factor which does

not depend on the object. The simplest way to introduce $\Delta\phi$ is to change the injection current. This leads to a small charge Δk_0 in wavevector (of the order of Δk) and hence $\Delta\phi = 2(\Delta k_0)l$.

In order to discuss the ability of the system to perform surface profilometry we begin by considering the signal from a perfect reflector. If we introduce defocus of u optical co-ordinates it is easy to calculate from Eqs. (5) and (6) that

$$U = \exp\left(-2jk_0 z\cos^2\frac{\alpha}{2}\right)\mathrm{sinc}\left(\frac{u}{2}\right), \tag{15}$$

where $\mathrm{sinc}(z) = \sin(z)/z$. It is easy to see that $\mathrm{Arg}\{U\}$ is proportional to z and so a feedback system which tracks variations in $\mathrm{Arg}\{U\}$ will provide a surface profile.

Although this shows that the system will produce a surface profile it does not say anything about the spatial resolution which might be obtained. In order to do this we will consider a specimen of uniform reflectivity but with a step in surface height of h at $x=0$. We shall further assume that h is sufficiently small that the microscope remains in focus on both sides of the step. It is then very straightforward to obtain an expression for $\mathrm{Arg}\{U\}$. The analysis is described in detail elsewhere [9] and so here we shall simply quote the expression for the confocal amplitude image $U(t)$

$$U(t) = \exp(-jk_0h')[\cos k_0h' - 2jf(t)\sin k_0h'], \tag{16}$$

where $h' = h\cos^2\alpha/2$ and

$$f(t) = \frac{1}{\pi}\int_0^2 \frac{c(m)}{m}\sin mt\,\mathrm{d}m, \tag{17}$$

where t is a normalised optical co-ordinate which is related to actual distance x, via $t = k_0 x\sin\alpha$. The function $c(m)$ is the in-focus coherent transfer function which is given [11,13] by

$$c(m) = \frac{2}{\pi}\left\{\cos^{-1}\left(\frac{m}{2}\right) - \frac{m}{2}\sqrt{1-\left(\frac{m}{2}\right)^2}\right\}. \tag{18}$$

It is now straightforward from Eq. (16) to write

$$\mathrm{Arg}\{U\} = k_0h' + \tan^{-1}\{2f(t)\tan k_0h'\}. \tag{19}$$

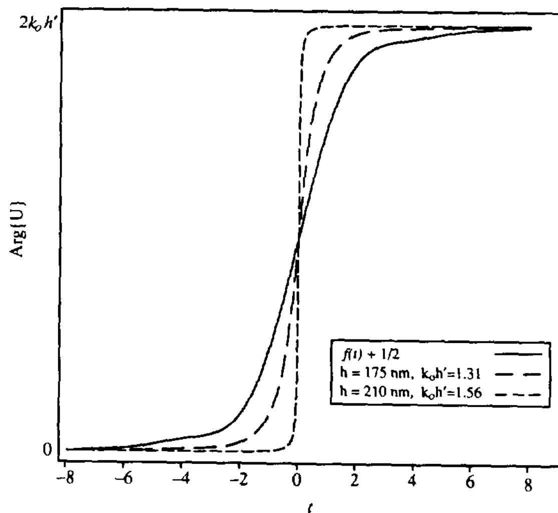

Fig. 2. The spatial variation in $\mathrm{Arg}\{U\}$ for different heights of step. The responses shown are for very small step heights (solid line), 175 nm and 210 nm step heights.

There are two simple limiting forms of this expression. The first is when the step height is such that tan k_0h' is sufficiently small to permit us to write

$$\mathrm{Arg}\{U\} = 2k_0h'[1/2 + f(t)], \tag{20}$$

which is proportional to the step height, h, with a spatial resolution determined by $1/2 + f(t)$. This function is plotted in Fig. 2 (solid line) and reveals a resolution as measured by the 20–80% width, of $0.38\lambda/\sin\alpha$ or 0.6 μm at 788 nm wavelength and a 0.5 NA objective lens. It is worth bearing in mind that the image of a straight edge object in a confocal microscope is given [13] by $[1/2 + f(t)]^2$ and hence the resolution we have just determined for the phase step is of the same order.

If we now consider phase steps such that k_0h' approaches $\pi/2$ then we see that $\tan k_0h' \to \infty$. We further recall that $f(t)$ is a smoothly varying function which tends to $-1/2$ as $t \to -\infty$ and $+1/2$ as $t \to +\infty$. This permits us to write

$$\mathrm{Arg}\{U\} \sim \frac{\pi}{2}\{1 + \mathrm{sgn}(t)\}, \tag{21}$$

where $\mathrm{sgn}(t) = 1(t>0)$ and $-1(t<0)$. This function has an extremely sharp transition at $t=0$, and gives the impression that super-resolution may be achieved [14,15]. However this is not really the case and arises, essentially, because of the nonlinear form of Eq. (19).

The function of fundamental importance is the image amplitude, U, and the spatially varying part of this is $f(t)$ which does not exhibit super-resolution. Fig. 2 shows the phase images for a variety of step heights where $0<k_0h'<\pi/2$. It is clear that great caution should be excerised in quantifying the resolution of such images. We further note that if we consider step heights in the region $\pi/2<k_0h'<3\pi/2$ then we find, Eq. (19), that the phase tends to a maximum as $t\to -\infty$ and zero as $t\to +\infty$, i.e. the opposite behaviour to that shown in Fig. 2.

We have now suggested a method to obtain $\mathrm{Arg}\{U\}$ and so it now merely remains to obtain $|U|$. This may be obtained, in principle, from our demodulated signals or by using a more sophisticated modulation feedback technique [9]. However there are problems in practice if the specimen feature height changes too rapidly. In a semiconductor laser implementation on the other hand we can avoid these problems altogether by simply reducing the injection current to the point when the coherence length is too short to allow interference to take place between the object and reference beams. In this case Eq. (1) takes the form

$$I=|r|^2+|U|^2 \tag{22}$$

from which the confocal signal $|U|^2$ can be readily obtained.

3. Experimental

The key elements of our experimental arrangement are shown in Fig. 1. Light from a single frequency semiconductor laser (Sharp LT021MD, 20 mW, 788 nm wavelength) was passed through a polarising beam splitter into a single mode optical fibre (York SM600). Light was then coupled into the confocal microscope from the distal end of the fibre. Since we did not index match the output end of the fibre, the light reflected from it formed the reference beam. The object scanning was achieved by mechanical scanning in the x and y directions whereas a piezoelectric bimorph was used for the z-scan to obtain the axial responses. A 0.5 numerical aperture Leitz objective lens was used throughout. The confocal amplitude signal travelled back along the fibre together with the reference beam and these were finally allowed to interfere on the photodetector. The purpose of the polarization controller was to ensure that the light coupled to the microscope was circularly polarized with the result that the reflected signals, after passing through the fibre, were polarized orthogonally to the laser waveform and were completely reflected by the beamsplitter towards the photodiode. The input end of the fibre was also cleaved at 10°. In these ways we endeavoured both to maximize the image signal and to reduce laser feedback effects.

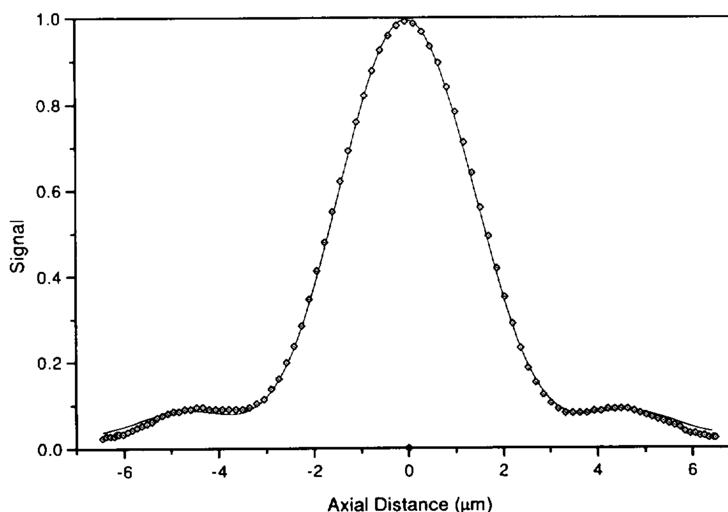

Fig. 3. The axial response as a planar reflector is scanned through focus The diamonds shows the experimental results and the solid line the theoretical fit.

We began by confirming that at a sufficiently low injection current the system behaved as a non-interference confocal microscope. In order to do this we mounted a planar reflector on the piezoelectric bimorph and measured the detected signal as we scanned the mirror through focus. The threshold injection current was found to be 47 mA and the axial response of Fig. 3 was obtained by operating the laser with an injection current of 52 mA. This value was chosen since it provided an adequate signal to noise ratio and the system did not show any interference effects. We note that our previous analysis, Eq. (15), was based on an ideal confocal microscope with an infinitely small point detector. In practice we used a single mode optical fibre and it is important to include the effects of the finite mode size into our theory. Fortunately this is very

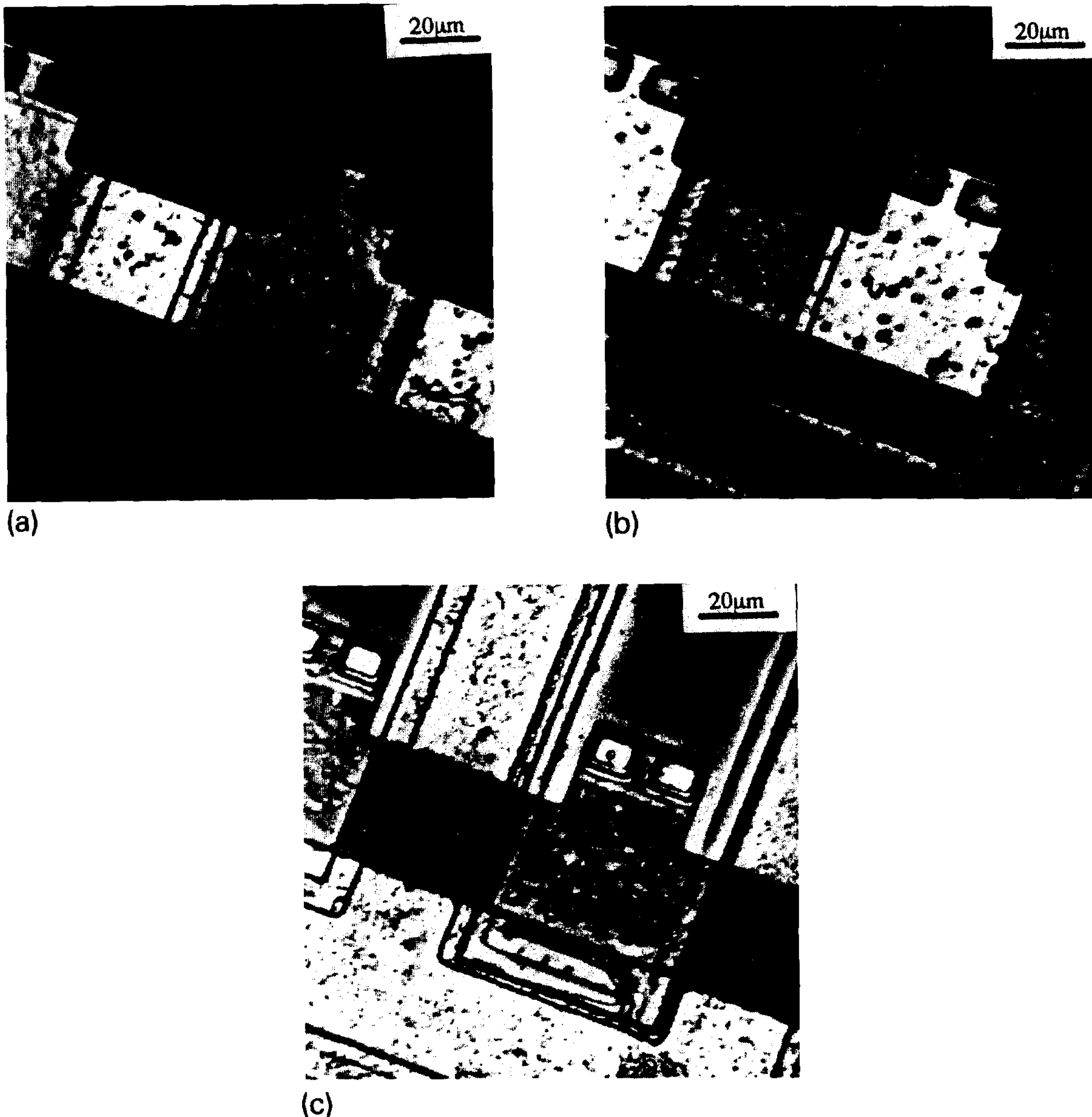

Fig. 4. Confocal images of a semiconductor chip, taken at three different axial positions. Relative to image (a), image (b) is axially displaced by 1.51 μm and image (c) by 2.56 μm in the same direction.

FULL LENGTH ARTICLE

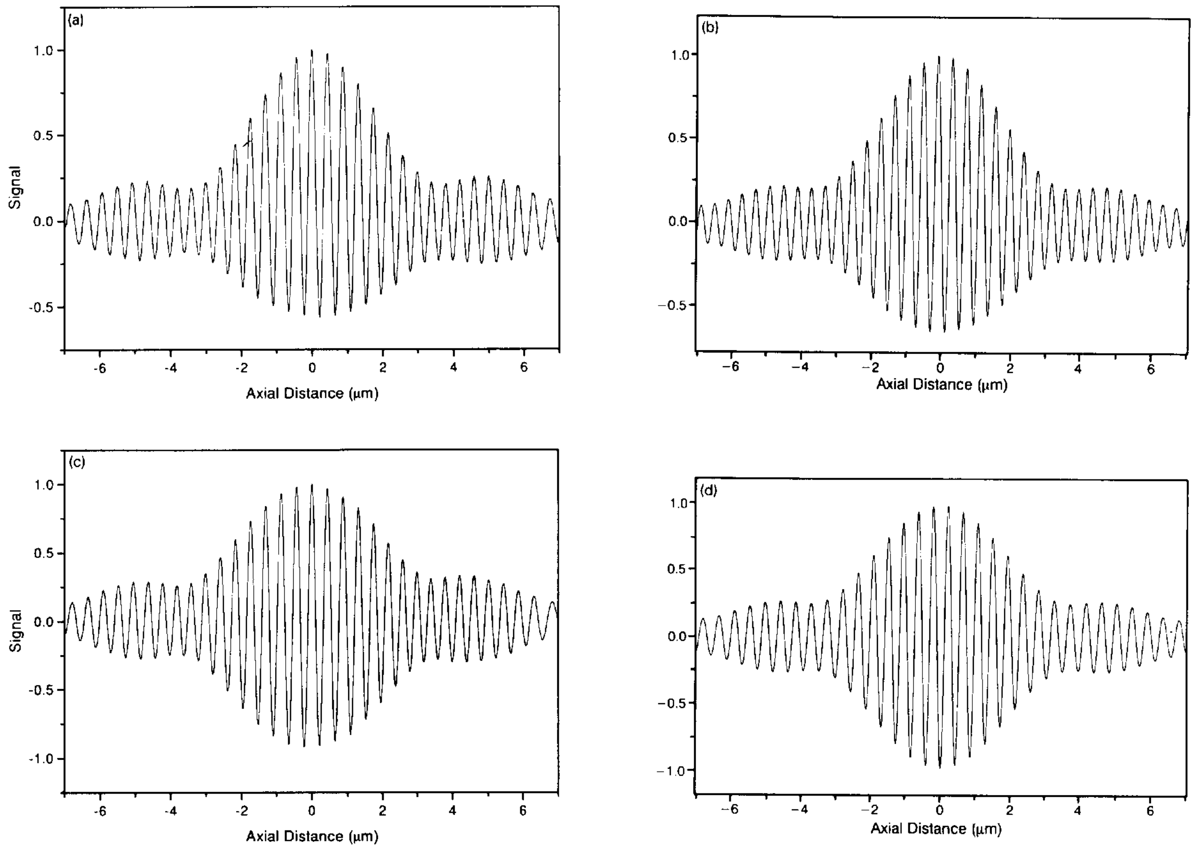

Fig. 5. The demodulated axial responses from the interference microscope. (a), (b) Experimental and theoretical curves corresponding to demodulation at 200 kHz. (c), (d) Experimental and theoretical results for demodulation at 400 kHz. In all cases the curves are normalised such that $I(0) = 1.0$ and the free parameter $a = 3.49$.

straightforward [16]. If we assume that the eigenmode can be described as a Gaussian of the form $\exp(-r^2/a^2)$ where a effectively describes the relative size of the eigenmode with respect to the point spread function then [16]

$$U = \exp\left(-2jk_0 z \cos^2\frac{\alpha}{2}\right)\operatorname{sinc}\left(\frac{u}{2} + \frac{ja}{4}\right) \tag{23}$$

and ideal confocal operation results as $a \to 0$. The smooth line in Fig. 3 shows a theoretical fit using $|U|^2$ from Eq. (23). We allowed both a and the numerical aperture to be free parameters. The best fit was obtained for $a = 3.49$ and a numerical aperture of 0.47 rather than the nominal value of 0.5. Fig. 4 shows a through focus series of images of a portion of a microcircuit to confirm that high quality non-interference confocal images may be obtained with the system.

In order to achieve interferometric phase imaging it was necessary to increase the injection current. We found a value of 69 mA to be adequate although its exact value was not critical. This value also permitted us to superimpose a 200 kHz modulation to provide the required phase modulation. We found that an injection current modulation of 0.33 mA led to $\Delta k \sim 2 \times 10^{-5}$ μm which translates to a phase modulation $\phi_0 = 2(\Delta k)l \approx 2\pi$. We used this level of injection current modulation since it produced a sufficiently high demodulated signal, $I_{2\omega}$. The other effect of injection current modulation is that the laser intensity is also modulated. For 0.33 mA modulation we measured $\beta = 0.015$.

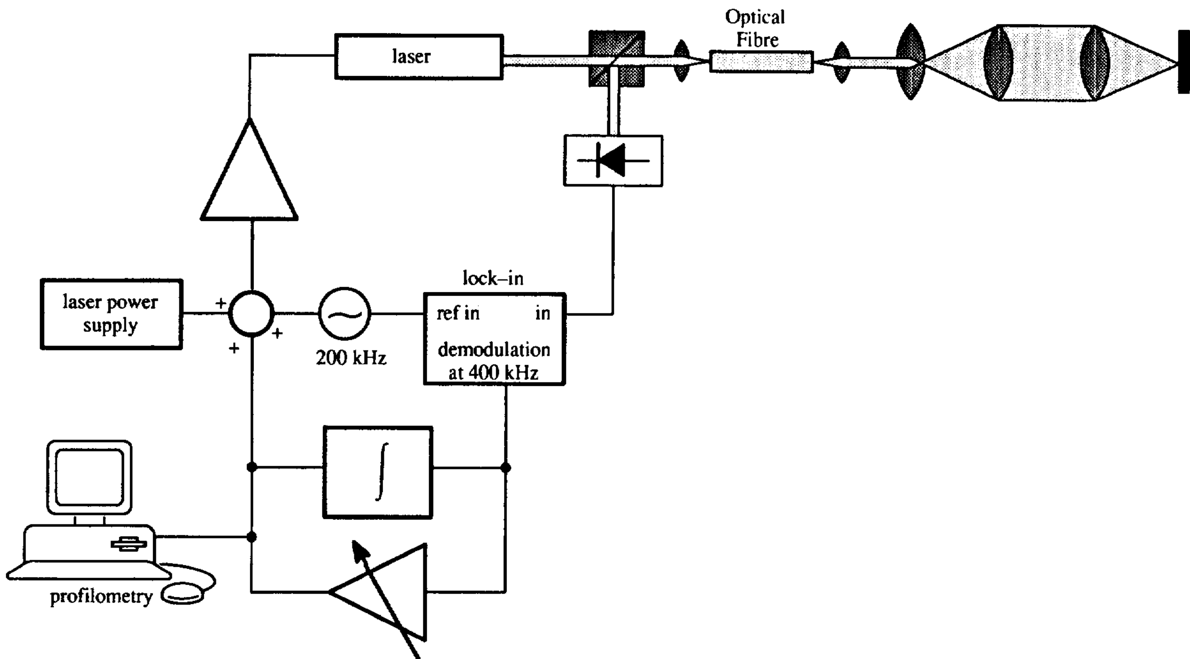

Fig. 6. Schematic diagram of the demodulation and feedback system.

Fig. 5 shows the axial responses demodulated at 200 kHz and 400 kHz together with the theoretical predictions according to Eqs. (11), (13) and (15). In order to obtain agreement in the 200 kHz demodulated case it was necessary to allow r, to be a free parameter. A value of $r = 0.78$ was found to be satisfactory.

In order to obtain the phase (height) image we used the 400 kHz demodulated signal as an error signal in a simple proportional plus integral feedback loop. The feedback signal was finally applied to the injection current such that the overall action of the system was to add an extra phase, $\Delta\phi$, Eq. (14), such that the demodulated term became zero. In this way the feedback signal represents the height profile and was available for surface profilometry, Fig. 6.

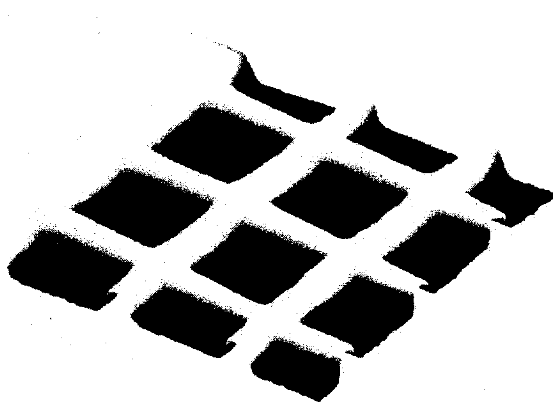

Fig. 7. Surface profile of a silicon test object. The lattice is 186 nm high and has period 10 μm.

We note that it is not possible to use the 200 kHz demodulated signal as the error signal since the form of this signal depends on the object reflectivity and this will vary from picture point to picture point. Thus introducing an extra phase term in a feedback to set I_ω, Eq. (11), equal to zero will not, in general, produce a surface profile.

Fig. 7 and 8 show two examples of surface profiles obtained with this system. Fig. 7 shows a silicon test specimen (Agar Scientific S1934) containing a pattern formed by electron beam lithography. The lattice period is 10 μm and the feature height is 186 nm ($k_0 h \cos^2\alpha/2 = 0.44\pi$). Fig. 8, on the other hand, shows a 90 μm square area of an etched aluminium pattern. The feature height is 12 nm ($k_0 h \cos^2\alpha/2 = 0.028\pi$).

These specimens were chosen both to demonstrate the sensitivity of our technique and to illustrate the

'super-resolution' that may be obtained in phase imaging when the step height is near $\lambda/4$. Fig. 9 shows the experimental line scans over edges in the two specimens as dots (186 nm step) and diamonds (12 nm step) together with theoretical fits determined by Eq. (19) superimposed and showing excellent agreement in both cases. We find that the resolution, as measured between the 20–80% intensity values is 0.6 μm for the 12 nm high edge which agrees with the limiting theoretical value ($0.8\ \lambda/\sin\alpha$). The resolution in the 186 nm high case on the other hand, Fig. 9a, is 0.2 μm. We attribute this apparent 'super-resolution' to the inherently nonlinear nature of phase imaging.

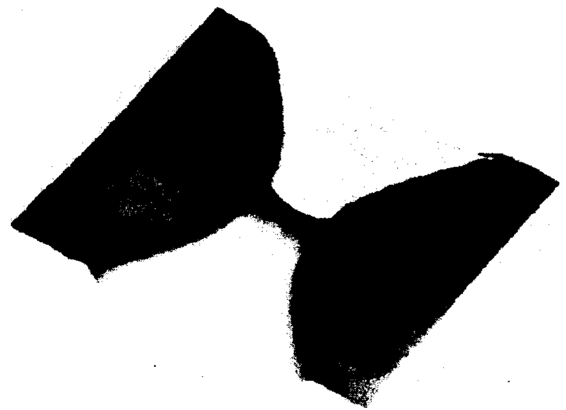

Fig. 8. The surface profile of a pattern in aluminium. The pattern is 12 nm high and the area shown is 90 μm square.

4. Conclusions

We have built a semiconductor laser based confocal scanning microscope which can image as a non-interference microscope when the injection current is low. On the other hand interference imaging results if the injection current is increased. A simple injection current modulation technique has been introduced which permits the interference term image to be extracted from the full interference image. Finally a feedback system has been finally introduced which allows us to determine the argument (phase) of the confocal amplitude image. This phase image has been used to produce high resolution surface profiles. However care should be taken in interpreting the spatial resolution of phase images since the imaging process is necessarily nonlinear. This leads to apparent higher spatial resolutions at step heights near to $\lambda/4$.

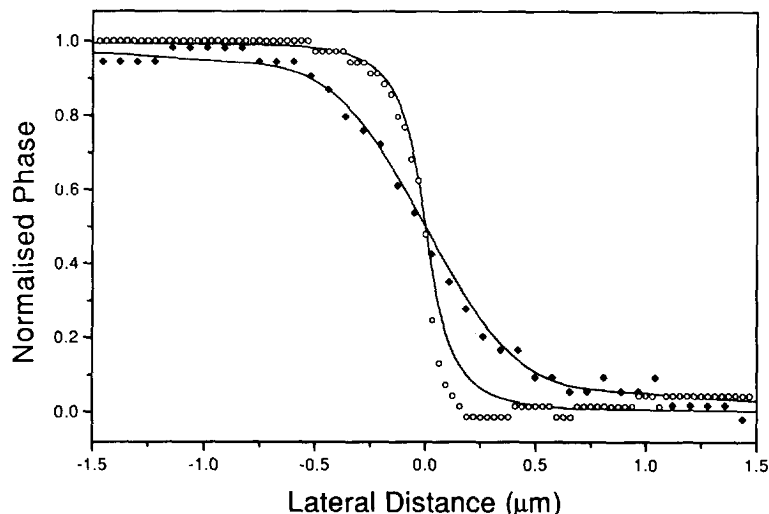

Fig. 9. Experimental and theoretical (solid lines) line scans across two phase edges. The dots correspond to a step height of 12 nm ($k_0h' = 0.028\pi$) and the diamonds to a step height of 186 nm ($k_0h' = 0.44\pi$). The increased sharpness of the response when the step height approaches $\pi/2$ is readily seen.

References

[1] R. Juškaitis and T. Wilson, Optics Comm. 92 (1992) 315.
[2] R. Juškaitis, F. Reinholz and T. Wilson, Electron. Lett. 28 (1992) 986.
[3] R. Juškaitis, N. Rea and T. Wilson, Optics Comm. 99 (1993) 105.
[4] R. Juškaitis, N.P. Rea and T. Wilson, Appl. Optics 33 (1994) 578.
[5] T. Wilson and R. Juškaitis, Bioimaging 2 (1994) 36.
[6] R. Juškaitis and T. Wilson, J. Microsc. 176 (1994) 188.
[7] A. Bearden, M.P. O'Neill, L. Osborne and T.L. Wang, Optics Lett. 18 (1993) 238.
[8] R. Juškaitis, T. Wilson and N.P. Rea, Optics Comm. 109 (1994) 167.
[9] K. Tatsuno and Y. Tsunoda, Appl. Optics 26 (1987) 37.
[10] T. Wilson, R. Juskaitis, N.P. Rea and D.K. Hamilton, Optics Comm. 110 (1994) 1.
[11] T. Wilson, ed., Confocal Microscopy (Academic Press, London, 1990).
[12] M. Abramowitz and I.A. Stegun, Handbook of Mathematical Functions (Dover, 1965).
[13] T. Wilson and C.J.R. Sheppard, Theory and Practice of Scanning Optical Microscopy (Academic Press, London, 1984).
[14] V.P. Tychinski, Optics Comm. 74 (1989) 41.
[15] M. Totzeck and M.A. Krumbugel, Optics Comm. 112 (1994) 189.
[16] T. Wilson, J. Opt. Soc. Am. 10 (1993) 1535.